

Millimeter-level resolution through-the-wall radar imaging enabled by an optically injected semiconductor laser

GUANQUN SUN, FANGZHENG ZHANG,*  AND SHILONG PAN 

Key Laboratory of Radar Imaging and Microwave Photonics, Ministry of Education, Nanjing University of Aeronautics and Astronautics, Nanjing 210016, China

*Corresponding author: zhangfangzheng@nuaa.edu.cn

Received 30 August 2021; revised 18 October 2021; accepted 19 October 2021; posted 26 October 2021 (Doc. ID 441803); published 9 November 2021

Millimeter-level resolution through-the-wall radar (TWR) imaging is demonstrated using a broadband nonlinear frequency-modulated (NLFM) signal that is generated by an optically injected semiconductor laser. The proposed system uses period-one dynamics of a semiconductor laser, together with an optical frequency downconversion technique to generate NLFM signals, which addresses the problem of traditional period-one oscillation not being able to generate broadband signals in the low-frequency region. In the experiment, an NLFM signal having a broad bandwidth of 18.5 GHz (1.5–20 GHz) is generated with a corresponding radar range resolution of 8.1 mm. Using this signal, TWR imaging is demonstrated, in which the use of the NLFM signal achieves good side-lobe suppression during pulse compression, and a modified back projection imaging algorithm with sub-aperture weighting is proposed to improve the imaging quality. © 2021 Optical Society of America

<https://doi.org/10.1364/OL.441803>

Through-the-wall radar (TWR) imaging has important applications in urban area detection, disasters rescue, and anti-terrorism, etc. [1]. A TWR usually transmits low-frequency electromagnetic waves that have good penetration capability to detect the targets behind obstacles [2]. To achieve high-resolution detection and imaging, a large bandwidth of the TWR is highly desired. However, the generation and processing of broadband low-frequency signals using traditional electronic devices or subsystems are still challenging. In recent years, various methods using photonic technologies to generate and process broadband radar signals have been proposed [3–9]. Among these methods, signal generation using period-one oscillation of an optically injected semiconductor laser has attracted a lot of attention because of its compact structure and good flexibility [10]. Previously, photonics-based radars with a centimeter-level range resolution have been demonstrated using broadband linear frequency-modulated (LFM) waveforms generated by period-one oscillations of a semiconductor laser [11]. However, it is difficult to generate broadband radar signals in the low-frequency region using this method, especially when the signal covers multiple frequency bands. The reasons are as

follows. First, it is impossible to generate radio frequency (RF) signals lower than 5 GHz based on period-one dynamics of current commercial semiconductor lasers, because the required detuning frequency between the master laser and the slave laser is such small that the injection would easily fall into the injection locking or chaotic state. Second, the optical signal generated by period-one oscillation usually contains four-wave mixing (FWM) idlers, which makes it impossible to generate signals over a single octave. This phenomenon severely limits the bandwidth when generating signals in the low-frequency region. Therefore, the previously reported radar signal generation based on period-one oscillation of an optically injected semiconductor laser is not suitable for high-resolution TWR imaging.

In this Letter, to solve the above-mentioned problems, we propose a method to generate broadband frequency-swept radar signals with a low starting frequency based on the period-one oscillation of a semiconductor laser, together with an optical frequency downconversion technique, and demonstrate its applications in high-resolution TWR radar imaging. A nonlinear frequency-modulated (NLFM) signal is generated in the proposed system instead of LFM signals, which enables large side-lobe suppression after radar pulse compression. This is particularly favorable for TWR radar imaging because high side-lobe suppression is preferred to distinguish the false targets in the radar detection environment with obstacles. In addition, to improve the TWR imaging quality, an improved incoherent back projection (BP) imaging method using sub-aperture weighting is proposed based on our previous work in [12], which not only suppresses the high-energy artifacts and background interferences, but also ensures the information integrity of the targets in the final image. In the experiment, an NLFM signal with a bandwidth of 18.5 GHz (1.5–20 GHz) is generated with a theoretical radar range resolution of 8.1 mm. Using the generated signal, high-resolution and high-quality TWR imaging is implemented.

Figure 1 shows the schematic diagram of the proposed TWR system. The typical frequency-modulated signal generation scheme based on period-one oscillations mainly consists of a master laser ([ML], frequency: f_m), a slaver laser (SL, free-running frequency: f_s), an optical circulator (CIR), a

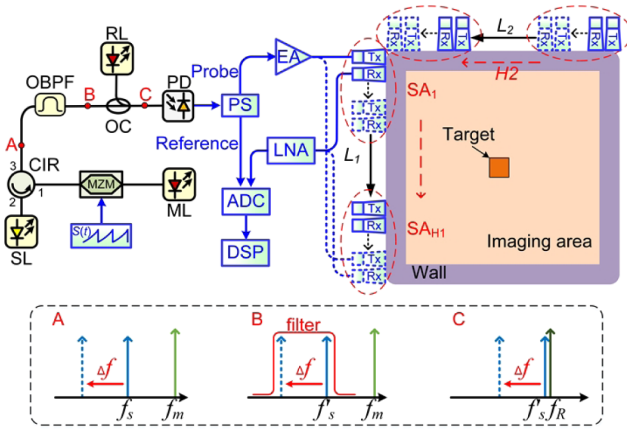


Fig. 1. Schematic diagram of the proposed TWR imaging system.

Mach-Zehnder modulator (MZM), and a photodetector (PD) [10]. The MZM is applied to vary the injection strength by performing optical intensity modulation of the ML. Under the period-one oscillation state, the optical signal at the output of the SL includes a regenerated optical carrier having the same frequency as the ML and a frequency-swept redshifted optical sideband (f'_i) [13]. For a given de-tuning frequency between the ML and the SL, by properly controlling the injection power, the frequency sweeping range of the red shifted sideband can be maximized. To avoid the spectral overlap between the FWM idlers and the redshifted optical sideband, the spectral spacing between the regenerated optical carrier and the redshifted sideband should be large enough. In previously reported schemes, this optical signal is converted to an electrical domain by a PD, and a frequency-modulated microwave signal is generated while, as explained above, a large bandwidth microwave signal can be generated only in the high-frequency region. To solve this problem, we use an optical bandpass filter (OBPF) to select the frequency-swept redshifted sideband, as shown in Fig. 1. The obtained optical signal is combined with the light from a reference laser (RL, frequency: f_r) by an optical coupler (OC) before being sent to a PD for optical-to-electrical conversion. The frequency of the RL is close to the redshifted sideband, and a frequency-modulated signal is generated after optical-to-electrical conversion at the PD. This way, the high-frequency P1 oscillation is downconverted to the low-frequency region. By designing the signal $S(t)$ that drives the MZM, the frequency modulation properties of the generated RF signal can be controlled [13]. Here we generate a Taylor weighted NLFM signal, of which the instantaneous frequency is [14]

$$f(t) = \frac{Bt}{T} + \sum_{m=1}^{\infty} K(m) B \sin\left(\frac{2\pi mt}{T}\right), \quad (1)$$

where B is the signal bandwidth, T is the pulse width, and $K(m)$ is m th order coefficient.

Afterwards, the generated NLFM signal is split into two branches by an electrical power splitter (PS). The signal in one branch is used as the reference for pulse compression. The signal in the other branch is amplified by an electrical amplifier (EA) and launched into the detection area by a transmit antenna (Tx). The radar echoes collected by the receive antenna (Rx) are amplified by a low-noise amplifier (LNA) and captured with the reference signal by a two-channel analog-to-digital converter

(ADC). To construct a 2D image, the Tx and Rx are moved together to form an equivalent synthetic aperture. Based on the signals collected at different observation positions, TWR imaging is implemented in a digital signal processor (DSP).

The incoherent BP algorithm is usually used for TWR image construction. In a traditional BP algorithm, pulse compression realized by matched filtering between the reference signal and the radar echoes is first implemented to obtain the range profiles $R_m(t_{ij})$ of different observation positions, where t_{ij} is the round-trip time delay between the m th observation position ($m = 1, 2, \dots, M$) and the image pixel at the coordinate of (x_i, y_j) . It should be noted that the thickness and dielectric constant of the wall or other obstacles should be considered in acquiring the accurate time delay [1]. Based on these range profiles, M coarse images can be obtained by assigning the amplitude of each pixel through interpolation [11]. Then all the coarse images are added up to get the final image. To improve the imaging quality, we proposed the incoherent BP imaging algorithm with self-amplitude weighting and multiplicative tomography weighting in [12], which effectively suppresses the high-energy artifacts and background interferences. However, in high-resolution TWR imaging, especially in near-field imaging scenarios, the use of multiplicative tomographic weighting proposed in [12] may result in loss of information because the amplitude contrast between different scattering points of the target may be excessively enlarged. To solve this problem, we propose a sub-aperture-weighting-based BP imaging method in this Letter. In this newly proposed method, the whole synthetic aperture is divided into H sub-apertures, and each sub-aperture is composed of K successive observation positions. Multiplicative tomographic weighting is applied in each sub-aperture to get H sub-images, and the H sub-images are accumulated to get the final image. The amplitude at the image pixel (x_i, y_j) is given by

$$A(x_i, y_j) = \sum_{b=1}^H \prod_{k=1}^K [R_{bk}(t_{ij})]^\alpha, \quad (2)$$

where the positive integer α is the multiplicative tomographic weighting factor.

To investigate the performance of the proposed TWR system, an experiment is conducted. In the experiment, the SL is a distributed feedback semiconductor laser (Actech LD15DM) that has a free-running wavelength of 1540.374 nm. It is biased at about seven times its threshold current. Both the ML and RL are generated by a multi-channel tunable laser (Agilent N7714A), of which the wavelength is 1540.19 and 1540.3637 nm, respectively. Figure 2(a) shows the optical spectra of the three lasers at a free-running state, which is measured by an optical spectral analyzer (Yokogawa AQ6370D) with a resolution of 0.02 nm. In Fig. 2(a), the RL and the SL have a small frequency spacing of about 1.5 GHz. An arbitrary waveform generator (Agilent 81150A; bandwidth: 120 MHz) generates the electrical control signal $S(t)$, which has a sawtooth profile with a period of 1.0 μ s and an amplitude of 3.9 V. It is used to modulate the light from the ML through an MZM (Lucent 2623NA; bandwidth: 10 GHz). After optical injection, the optical spectrum at the output of the SL is measured, as shown by the black dashed line in Fig. 2(b). As can be seen, a frequency-swept redshifted optical sideband is generated because of the period-one oscillation. The frequency sweeping range is about 0.1467 nm, corresponding

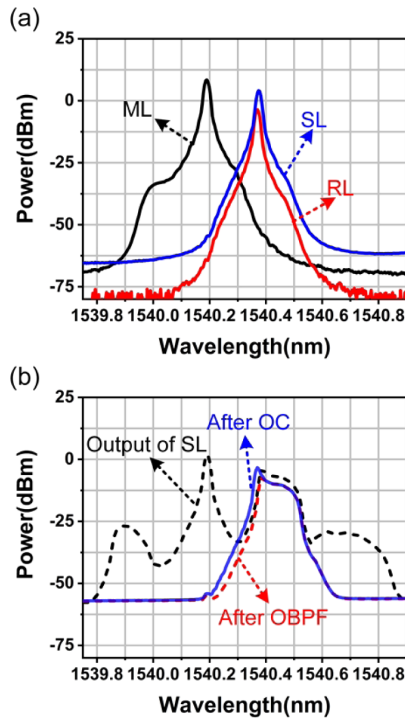


Fig. 2. (a) Measured optical spectra of the ML, RL, and free-running SL. (b) Measured optical spectra measured at the output of the SL (black dashed line) after the OBPF (red dotted line) and after the OC (blue solid line).

to a bandwidth of 18.5 GHz. In addition to the redshifted sideband, frequency sweeping FWM idlers are also observed. Fortunately, there is no spectral overlap between them, and the frequency-swept redshifted sideband is selected using an OBPF (Yenista XTM-50) with negligible interference from the FWM idlers. The optical spectrum measured after the OBPF is shown by the red dotted line in Fig. 2(b), in which the regenerated optical carrier and undesired FWM idlers are removed. Then the optical signal is combined with the RL, and the spectrum of the obtained optical signal after the OC is shown by the blue line in Fig. 2(b). After optical-to-electrical conversion at a PD (u2t XPDV2120RA, bandwidth: 40 GHz), a frequency sweeping electrical signal is generated, which covers a spectral range from 1.5 to 20 GHz. The obtained signal is close to an LFM signal, since the control signal $S(t)$ has a sawtooth profile. To generate an NLFM signal, the relationship between the instantaneous frequency and $S(t)$ is obtained and used to generate a modified control signal $S'(t)$ that leads to a frequency-time relation of an ideal NLFM signal [13]. In our experiment, the parameters of the ideal NLFM signal are set as $m = 7$ and $K(m) = [-0.1145, 0.0396, -0.00202, 0.00118, -0.00082, 0.0055, 0.0040]$.

The generated NLFM signal is sampled by a real-time oscilloscope (Keysight, DSO-X 92504A) with a sampling rate of 80 GSa/s. Figure 3(a) shows the waveform of the NLFM signal, and Fig. 3(b) shows the instantaneous frequency recovered by performing short-time Fourier transformation. In Fig. 3(a), amplitude fluctuations of the waveform, which are mainly caused by the different efficiencies of the period one oscillation at different frequencies, are observed. In practical applications,

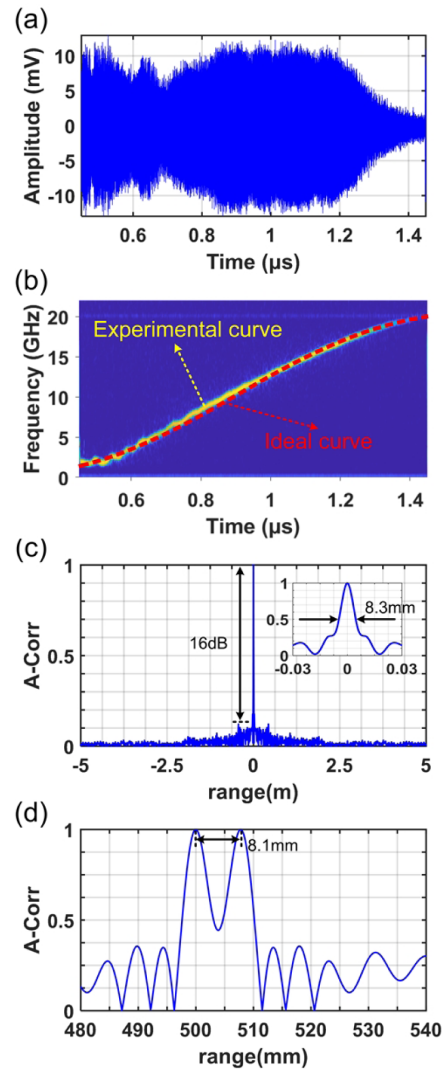


Fig. 3. (a) Measured waveform of the generated NLFM signal, (b) the recovered and ideal NLFM instantaneous frequency, (c) auto-correlation results of the signal (insets: the amplified autocorrelation peak), and (d) correlation between the transmitted and received waveforms.

this problem can be easily solved by using a wideband limiting amplifier. The result in Fig. 3(b) shows that the generated NLFM signal covers a broad bandwidth of 18.5 GHz (1.5–20 GHz), and the time-bandwidth product is calculated to be 1.85×10^4 . Besides, the time-frequency relationship of the NLFM signal is very close to that of the ideal NLFM signal.

To check the pulse compression property, autocorrelation of the generated NLFM signal is calculated and shown in Fig. 3(c). The peak to side-lobe ratio (PSLR) of the pulse after compression is 16 dB, which is close to the PSLR value (17.3 dB) of the ideal NLFM signal. It should be noted that, for an ideal LFM signal having the same bandwidth and temporal period, the PSLR after pulse compression is 12.4 dB. Hence, the use of the NLFM signal brings better side-lobe suppression for radar pulse compression. The zoom-in view in Fig. 3(c) shows the autocorrelation peak has a full width at half-maximum of 8.3 mm, which is close to the theoretical range resolution of 8.1 mm. To further check the range resolution, the NLFM signal and its

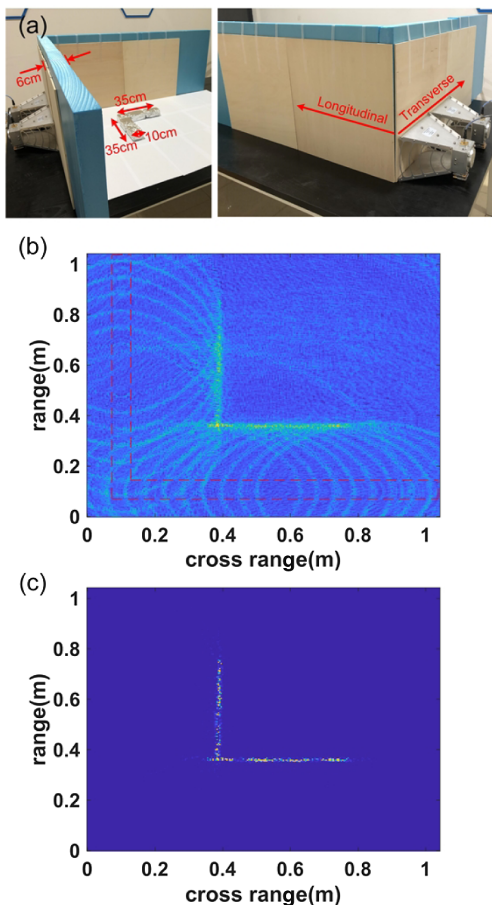


Fig. 4. (a) Photograph of the experimental scene and the images obtained by (b) a traditional BP algorithm and (c) improved sub-aperture weighting BP algorithm.

replica, which is optically delayed by 8.1 mm, are combined to imitate a two-target detection scenario. After matched filtering by performing a cross correlation between the reference NLFM signal and the equivalent radar echo, the peaks corresponding to the two targets are clearly distinguished, as depicted in Fig. 3(d). Thus, a millimeter-level range resolution of 8.1 mm is achieved by using the generated NLFM signal.

Finally, TWR imaging is demonstrated using the broadband NLFM signal. In the experiment, the wall is composed of two layers of wood with thick foam in the middle. The thickness of each layer of wood is 0.5 cm, and the thickness of the foam is 5 cm. Thus, the wall has a total thickness of 6 cm. Based on the electromagnetic properties of wood and foam, the dielectric constant of the wall is chosen as 2.8 in the TWR imaging process. The target blocked by the wall is an L shaped object consisting of four cubic reflectors, as shown in Fig. 4(a). In order to increase the reflection intensity, each reflector is wrapped by tin foil. The transmit antenna and receive antenna are attached to the wall and move simultaneously along the transverse and longitudinal directions to detect the area inside the wall. The size of the synthetic aperture in both directions is 35.36 cm with 12 equally spaced observation positions. Based on the received radar echoes, a traditional BP algorithm is first applied to construct the image. In the results shown in Fig. 4(b), the areas

corresponding to the wall are marked with red dashed lines. It is found that, due to the change of the dielectric constant in the wall area, irregular bending of the elliptical tracks is observed. Thanks to the high range resolution of the radar, the general shape of the target can be easily observed in Fig. 4(b), although high-energy artifacts and background interferences are serious. When the imaging method based on Eq. (2) is used, in which the synthetic aperture is divided into four sub-apertures in both directions and the value of α is chosen as 3, the constructed image is shown in Fig. 4(c). It is obvious that the target in Fig. 4(c) is well focused, and the artifacts and interferences are effectively suppressed. Therefore, high-resolution and high-quality image is successfully generated by the use of the broadband NLFM, signal as well as the modified incoherent BP imaging method.

In conclusion, we have proposed a method for generating broadband NLFM signals and demonstrated its application in TWR imaging in which the range resolution reaches 8.1 mm. It should be mentioned that, by further optimizing the detuning frequency and the dynamic range of the injected optical power, the bandwidth of the generated signal is expected to be further increased, enabling a higher range resolution towards 1 mm. Due to the hardware constraint, single-polarization receiving is used in the experiment. If a dual-polarization receiving scheme is adopted, the signal-to-noise ratio, as well as the imaging quality, can be improved.

Funding. National Natural Science Foundation of China (61871214); Natural Science Foundation of Jiangsu Province (BK20180066).

Disclosures. The authors declare no conflicts of interest.

Data Availability. Data underlying the results presented in this paper are not publicly available at this time but may be obtained from the authors upon reasonable request.

REFERENCES

- M. G. Amin and F. Ahmad, *IEEE Signal Process. Mag.* **25**(4), 110 (2008).
- C. Zhang, Y. Kuga, and A. Ishimaru, *IEEE Trans. Antennas Propag.* **66**, 4240 (2018).
- P. Ghelfi, F. Laghezza, F. Scotti, G. Serafino, A. Capria, S. Pinna, D. Onori, C. Porzi, M. Scaffardi, A. Malacarne, V. Vercesi, E. Lazzeri, F. Berizzi, and A. Bogoni, *Nature* **507**, 341 (2014).
- R. Li, W. Li, M. Ding, Z. Wen, Y. Li, L. Zhou, S. Yu, T. Xing, B. Gao, Y. Luan, Y. Zhu, P. Guo, Y. Tian, and X. Liang, *Opt. Express* **25**, 14334 (2017).
- S. Peng, S. Li, X. Xue, X. Xiao, D. Wu, X. Zheng, and B. Zhou, *Opt. Express* **26**, 1978 (2018).
- F. Zhang, Q. Guo, and S. Pan, *Sci. Rep.* **7**, 13848 (2017).
- W. Zou, H. Zhang, X. Long, S. Zhang, Y. Cui, and J. Chen, *Sci. Rep.* **6**, 19786 (2016).
- F. Zhang, Q. Guo, Z. Wang, P. Zhou, G. Zhang, J. Sun, and S. Pan, *Opt. Express* **25**, 16274 (2017).
- F. Zhang, B. Gao, and S. Pan, *Opt. Express* **26**, 17529 (2018).
- P. Zhou, F. Zhang, Q. Guo, S. Li, and S. Pan, *IEEE J. Sel. Top. Quantum Electron.* **23**, 1 (2017).
- G. Sun, F. Zhang, and S. Pan, *Opt. Commun.* **466**, 125633 (2020).
- G. Sun, F. Zhang, and S. Pan, in *IEEE MTT-S International Wireless Symposium (IWS)* (2019), pp. 1–3.
- P. Zhou, F. Zhang, Q. Guo, and S. Pan, *Opt. Express* **24**, 18460 (2016).
- I. S. Merrill, *Radar Handbook*, 3rd Ed. (McGraw-Hill Education, 2008).